Small-signal modeling of GaN HEMT switch with a new intrinsic elements extraction method

Miao Geng(耿苗)[1,2], Pei-Xian Li(李培咸)[1], Wei-Jun Luo(罗卫军)[2], Peng-Peng Sun(孙朋朋)[2], Rong Zhang(张蓉)[1,2], and Xiao-Hua Ma(马晓华)[1,†]

[1] *School of Advanced Materials and Nanotechnology, Xidian University, Xi'an* 710071, *China*

[2] *Key Laboratory of Microelectronics Devices & Integrated Technology, Institute of Microelectronics, Chinese Academy of Sciences, Beijing* 100029, *China*

(Received 6 July 2016; revised manuscript received 10 August 2016; published online 28 September 2016)

A novel and accurate method is proposed to extract the intrinsic elements of the GaN high-electron-mobility transistor (HEMT) switch. The new extraction method is verified by comparing the simulated *S*-parameters with the measured data over the 5–40 GHz frequency range. The percentage errors E_{ij} within 3.83% show the great agreement between the simulated S-parameters and the measured data.

Keywords: GaN high-electron-mobility transistor switch, small signal modeling, parameter extraction, error percentage

PACS: 73.61.Ey, 85.30.De, 85.40.Bh, 84.40.–x **DOI:** 10.1088/1674-1056/25/11/117301

1. Introduction

Radio frequency (RF) switches play an important role in modern communication systems such as mobile base station transceivers and satellite communication transmitters. Currently, the two most widely used microwave and RF semiconductor components in switches are PIN diodes and GaAs metal–semiconductor field effect transistors (MESFETs).[1] The traditional PIN diode based T/R switches encounter additional losses as a result of their intrinsic DC power consumption. The GaAs FET-based switches are hampered by the relatively low breakdown voltage of the components, which require multi-stage design configurations with active device series connections to divide the maximum voltage of the input signal.[2] The GaN on silicon carbide (SiC) HEMT technology offers many advantages over the existing GaAs technology.[3–5] Because of its higher breakdown voltage, GaN promises to extend the power level of the FET-based microwave circuits by at least a factor of five.[6–8] The greatly increased breakdown voltage ($V_{\rm BD}$) will allow the use of a higher control voltage and correspondingly larger RF voltage swings for off-state transistors. The high maximum current capability ($I_{\rm MAX}$) reduces the channel resistance and increases the RF current swing for on-state devices. The insulating SiC substrate reduces the substrate leakage due to the high RF voltage swing and improves heat transfer to the backside of the MMIC.[9] Furthermore, GaN HEMT switches can provide low insertion loss and high switching speed performance with minimal dc-bias power needed for the switching action. It also enables excellent small and large signal performances over a wider frequency band. This has positioned the GaN HEMT based RF switches as the natural replacement for the Si PIN diode or GaAs PHEMT switches with more application space to be explored.

Over the last few decades, the development of an accurate device model has proven to be a vital step in the "first pass" design approach. As we know, an accurate extraction method for a proper small-signal equivalent circuit is vital for designing circuits, evaluating the process technology, and optimizing the device performance. However, modeling switches is not as extensively covered in some previous literatures as that of a power amplifier (PA). Also, switches usually operate at passive mode and in practice in a common gate (CG) configuration, which is different to the familiar common source (CS) model.[10] So far, there is almost no detailed extraction procedure for the GaN HEMT switch model in the previous publications.

We propose a new method for the extraction of the intrinsic elements in the GaN HEMT switch and describe the whole extraction procedure of elements in the GaN HEMT switch model. In Section 2, the device structure is presented. The detailed extraction procedure of the extrinsic and intrinsic elements is described in Section 3. In Section 4, the results and validity of the proposed small-signal modeling procedure are discussed. Finally, some concluding remarks are given in Section 5.

2. Device structure

The GaN based HEMT switch employed in this work is grown on a SiC substrate as shown in Fig. 1. The process of metal organic chemical vapor deposition (MOCVD) is used in order to grow an AIN spacer layer, an AlGaN barrier layer, and a GaN layer on the substrate. Ohmic contacts are created

†Corresponding author. E-mail: xhma@xidian.edu.cn

© 2016 Chinese Physical Society and IOP Publishing Ltd

by depositing Ti/Al/Ni/Au metals followed by rapid thermal annealing at a high temperature (870 °C) in nitrogen gas. A passivation layer of silicon nitride (SiN) with a thickness of 2000 Å is deposited by using a plasma enhanced chemical vapor deposition (PECVD) system. The spacing between the source and the drain is 3.5 μm. The gate length and width of the device are 0.25 μm and 400 μm (100 μm×4), respectively. The top-view photograph of the GaN HEMT switch with gate size of 4×100 μm is shown in Fig. 2.

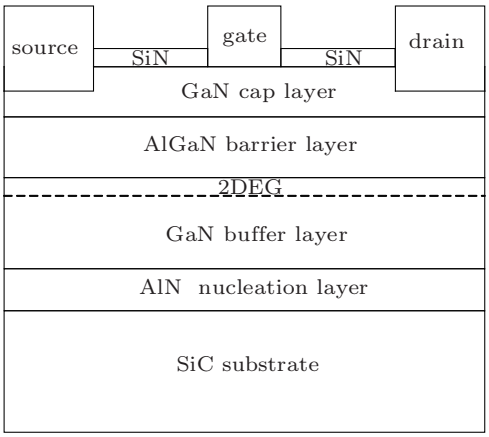


Fig. 1. Cross-sectional structure of GaN based HEMT switch.

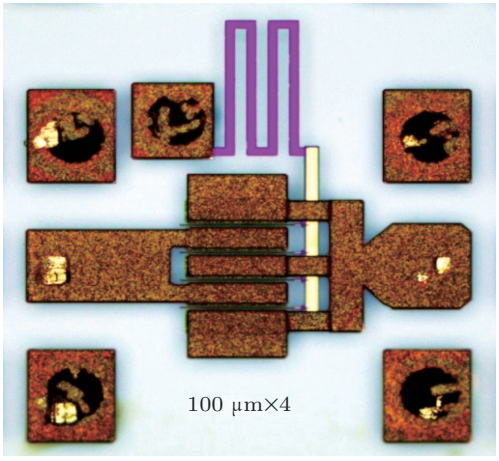


Fig. 2. (color online) GaN based HEMT switch with gate size of 4 × 100 μm.

3. Extraction procedure

Based on the physical properties, the schematic of the AlGaN/GaN HEMT equivalent circuit is shown in Fig. 3. The equivalent circuit of the GaN HEMT switch is the same for on state (V_{ds} = 0 V, V_{gs} = 0 V) and off state (V_{ds} = 0 V, V_{gs} = −5 V).[11] The simulation of the circuit schematic is implemented using the advanced design system (ADS) software. The parameters in Fig. 3 can be divided into two parts. The parasitic part includes parasitic inductances and resistances at the source (L_s, R_s), drain (L_d and R_d), and gate (L_g and R_g) electrodes, as well as parasitic capacitors (C_{pg} and C_{pd}) induced by the package effect. We assume that the parasitic parameters are evaluated and de-embedded correctly, the remaining bias dependent intrinsic part consists of C_{gs}, C_{gd}, C_{ds}, and R_{ds}. Here C_{gs}, C_{gd}, and C_{ds} are the gate–source, gate–drain, and drain–source intrinsic capacitances, respectively;[12] R_{ds} is the channel resistance between the source and the drain. The two-part S parameter measurements for model extraction and verification at 40 GHz are carried out by using an Agilent E8363B PNA series network analyzer. All measurements are carried out on a wafer using SUSS PA200 probes station, with all instruments under IC-CAP software control. The measurements are performed with a 50-Ω characteristic impedance system. The following outlines the procedure for the correct extraction of the entire set of circuit elements.

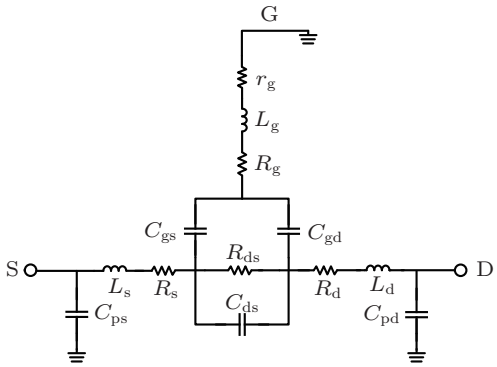


Fig. 3. Small signal equivalent circuit of GaN HEMT switch.

3.1. Extrinsic elements

Parasitic source and drain pad capacitances of GaN HEMT are generally extracted by the conventional cold pinch-off (V_{DS} = 0 V, $V_{GS} < V_p$) techniques. Under the condition $V_{GS} < V_p$, the channel between the source and the drain is completely pinched-off with the capacitive elements dominant. At low frequencies, the inductances and resistances can be neglected as they do not influence the imaginary part of the Y parameters. At V_{DS} = 0 V, the depletion layer under the gate is symmetric and this allows us to assume that C_{gs} and C_{gd} equal to C_g. Such an approximation depends on the symmetric structure of the switch device. Under this bias state, the equivalent-circuit topology of Fig. 4 is deemed to be an adequate electrical representation of the device under this condition.[13] The Y parameters of the complete device under the pinch-off bias condition can be written as

$$\mathrm{Im}(Y_{11}) = \mathrm{j}\omega\left(C_{ps} + \frac{2}{3}C_g\right), \tag{1}$$

$$\mathrm{Im}(Y_{12}) = \mathrm{Im}(Y_{21}) = -\mathrm{j}\omega\frac{2}{3}C_g, \tag{2}$$

$$\mathrm{Im}(Y_{22}) = \mathrm{j}\omega\left(C_{pd} + \frac{2}{3}C_g\right), \tag{3}$$

where $\mathrm{Im}(Y_{11})$, $\mathrm{Im}(Y_{12})$, $\mathrm{Im}(Y_{21})$, and $\mathrm{Im}(Y_{22})$ represent the imaginary part in Fig. 4, respectively.

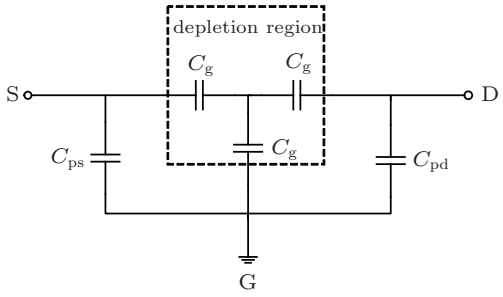


Fig. 4. Cold pinch-off equivalent circuit for GaN HEMT at low frequency.

The extracted parameters via Eqs. (2)–(4) are shown in Fig. 5. We obtain $C_{ps} \approx 41.3$ fF, $C_{pd} \approx 38.7$ fF and the difference between C_{ps} and C_{pd} is very small. The parasitic capacitance between the source and the drain is only a few fF and can be ignored.

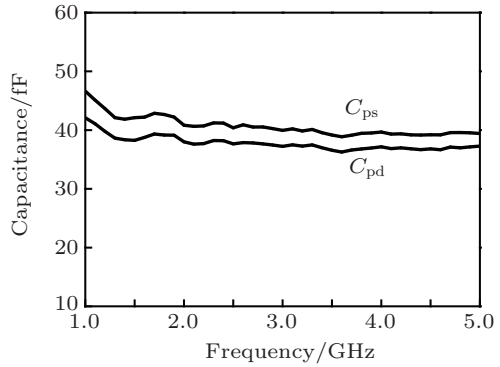


Fig. 5. Extracted pad capacitances against frequency.

After de-embedding the effect of the pad capacitances, the other six extrinsic elements can be determined from Z-parameters under no bias condition in Fig. 6 as follows:

$$Z_{11} = R_s + \frac{R_{ch}}{2} + R_g + r_g + \mathrm{j}\left[\omega(L_g + L_s) - \frac{1}{\omega C_g}\right], \quad (4)$$

$$Z_{12} = Z_{21} = R_g + r_g + \mathrm{j}\,\omega L_g - \frac{1}{\omega C_g}, \quad (5)$$

$$Z_{22} = R_d + \frac{R_{ch}}{2} + R_g + r_g + \mathrm{j}\left[\omega(L_g + L_d) - \frac{1}{\omega C_g}\right]. \quad (6)$$

As illustrated in Eqs. (4)–(6), inductances L_g, L_s, L_d are determined from the slopes of the straight lines approximating $\omega\mathrm{Im}(Z_{ij})$ versus ω^2. The parasitic resistances are evaluated by averaging the real part of Z-parameters in Eqs. (4)–(6) and the real part of Z_{11} under the pinch-off condition (the gate Schottky resistance R_g is far less than blocking resistor $r_g = 4$ kΩ, which can be ignored) is

$$Z_{11} = R_s + r_g, \quad (7)$$

where $\mathrm{Re}[Z_{11}]$ represents the real part of Z_{11}.

Figure 7 shows the extracted results of the feed line inductances. It can be found that L_s and L_d are very close to each other and larger than L_g. The inductances are $L_s = 62.4$ pH, $L_d = 58.5$ pH, and $L_g = 5$ pH. Figure 8 shows the extrinsic resistances. It can be observed that the best frequency range for the extraction of the extrinsic inductances and resistances is beyond 25 GHz. The parasitic resistances become increasingly dominant with increasing frequency, whereas the capacitances become low impedances and tend to short circuit. That is why the real parts of Z-parameters are dominated in the high frequency range. Therefore, the extrinsic resistances have to be extracted in the high-frequency range. All the extracted parasitic elements are summarized in Table 1.

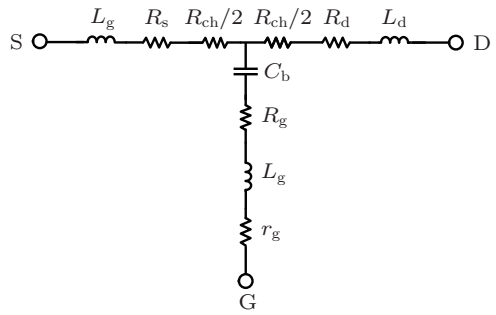


Fig. 6. Equivalent circuit for the GaN HEMT under no bias condition.

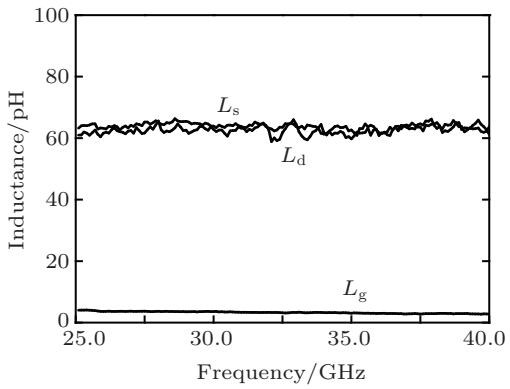


Fig. 7. Extracted feed line inductances against frequency.

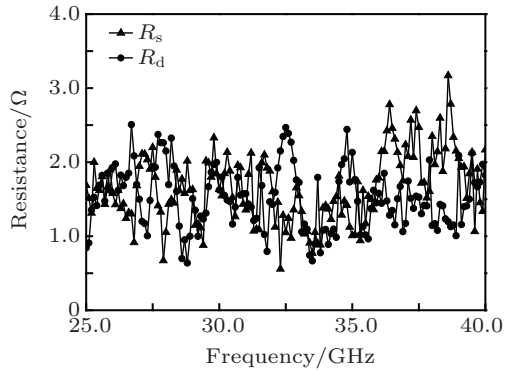


Fig. 8. Extracted extrinsic resistances against frequency.

Table 1. Extracted extrinsic elements of device with gate size of 4×100 μm.

C_{ps}/fF	C_{pd}/fF	L_s/pH	L_g/pH	L_d/pH	R_s/Ω	R_d/Ω	r_g/Ω
41.3	38.7	62.4	5	58.5	1.68	1.85	4 KΩ

3.2. Intrinsic elements

Usually, the Y parameters of common source devices satisfy $Y_{11} \neq Y_{12} \neq Y_{21} \neq Y_{22}$. There is only a small ohmic contact resistance between the source and the ground. After de-embedding all the parasitic parameters, the intrinsic part of the CS device can be obtained directly by the Y parameters of the two-part network. In the same way, for the CG GaN HEMT switch device, after de-embedding the extrinsic parameters, the intrinsic part is shown in Fig. 9(a). The intrinsic Y parameters of the GaN HEMT switch are usually characterized by the following equations:[14,15]

$$Y_{\text{int}} = \begin{bmatrix} \mathrm{j}\omega C_{\text{ds}} + \dfrac{1}{R_{\text{ds}}} + \dfrac{\mathrm{j}\omega C_{\text{gs}} C_{\text{gd}}}{C_{\text{gs}} + C_{\text{gd}}} & -\mathrm{j}\omega C_{\text{ds}} - \dfrac{1}{R_{\text{ds}}} - \dfrac{\mathrm{j}\omega C_{\text{gs}} C_{\text{gd}}}{C_{\text{gs}} + C_{\text{gd}}} \\ -\mathrm{j}\omega C_{\text{ds}} - \dfrac{1}{R_{\text{ds}}} - \dfrac{\mathrm{j}\omega C_{\text{gs}} C_{\text{gd}}}{C_{\text{gs}} + C_{\text{gd}}} & \mathrm{j}\omega C_{\text{ds}} + \dfrac{1}{R_{\text{ds}}} + \dfrac{\mathrm{j}\omega C_{\text{gs}} C_{\text{gd}}}{C_{\text{gs}} + C_{\text{gd}}} \end{bmatrix}. \tag{8}$$

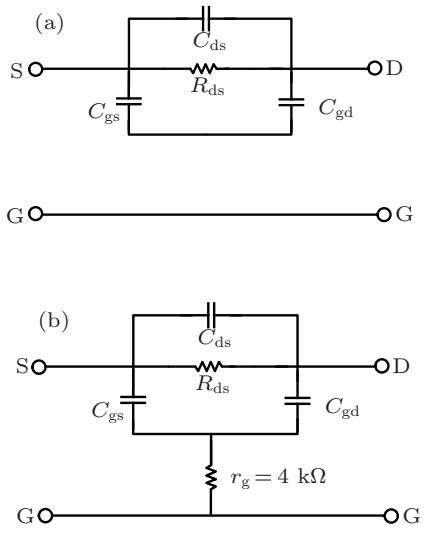


Fig. 9. The intrinsic part (a) without r_{g} and (b) with r_{g}.

The GaN HEMT under switch bias condition is passive, and hence, the condition $Y_{12} = Y_{21}$ is satisfied in Eq. (8). Furthermore, the common gate GaN HEMT switch device has a symmetrical geometry, which is reflected in the observation that $Y_{11} = Y_{22}$. However, the large blocking resistor on the gate makes the gate be an open circuit to the ground. As shown in Eq. (8), the Y parameters of the GaN HEMT switch device obtained by the traditional method satisfy $Y_{11} = Y_{22} = -Y_{12} = -Y_{21}$. So, there are only two equations but four unknown elements for the intrinsic parameters. Therefore, the traditional method cannot extract the intrinsic parameters of the GaN HEMT switch model.

So far, the previous literatures have not given any specific equations of the extraction method about the intrinsic parameters in switch models. Most of the intrinsic parameters were extracted by optimization or some algorithms.[16–21] Based on the problem mentioned above, a specific method and a detailed procedure of intrinsic parameters extraction are described as follows.

As shown in Fig. 9(b), after de-embedding parasitic capacitances C_{ps}, C_{pd}, extrinsic resistances R_{s}, R_{d}, and inductances L_{s}, L_{d}, L_{g}, the remaining part includes the blocking resistor r_{g} and intrinsic parameters R_{ds}, C_{ds}, C_{gs}, and C_{gd}. The gate of the GaN HEMT switch device is connected to the ground by a blocking resistor ($r_{\text{g}} = 4$ kΩ), which is used to decouple the circuit from the common gate ground.[22–24] In order to solve the problem in the traditional extraction method, the blocking resistor is taken into consideration during extracting the intrinsic elements, which is the first time parasitic elements have been used in the intrinsic elements extraction process. By using this new method, the Y parameters of the intrinsic part can be expressed as

$$Y_{\text{int}} = \begin{bmatrix} \mathrm{j}\omega C_{\text{ds}} + \dfrac{1}{R_{\text{ds}}} + \dfrac{1}{2r_{\text{g}} + \dfrac{1}{\mathrm{j}\omega C_{\text{g}}}} + \dfrac{1}{\dfrac{2}{\mathrm{j}\omega C_{\text{g}}} - \dfrac{1}{\omega^2 C g^2 r_{\text{g}}}} & -\mathrm{j}\omega C_{\text{ds}} - \dfrac{1}{R_{\text{ds}}} - \dfrac{1}{\dfrac{2}{\mathrm{j}\omega C_{\text{g}}} - \dfrac{1}{\omega^2 C g^2 r_{\text{g}}}} \\ -\mathrm{j}\omega C_{\text{ds}} - \dfrac{1}{R_{\text{ds}}} - \dfrac{1}{\dfrac{2}{\mathrm{j}\omega C_{\text{g}}} - \dfrac{1}{\omega^2 C g^2 r_{\text{g}}}} & \mathrm{j}\omega C_{\text{ds}} + \dfrac{1}{R_{\text{ds}}} + \dfrac{1}{2r_{\text{g}} + \dfrac{1}{\mathrm{j}\omega C_{\text{g}}}} + \dfrac{1}{\dfrac{2}{\mathrm{j}\omega C_{\text{g}}} - \dfrac{1}{\omega^2 C g^2 r_{\text{g}}}} \end{bmatrix}. \tag{9}$$

The Y parameters in matrix (9) satisfy the relationships $Y_{11} = Y_{22}$ and $Y_{12} = Y_{21}$. In order to simplify the extraction formula, based on the geometric structure of the GaN HEMT switch, i.e., the depletion layer under the gate is symmetric, it can be assumed that

$$C_{\text{gs}} = C_{\text{gd}} = C_{\text{g}}. \tag{10}$$

By combining Eqs. (9) and (10), the intrinsic elements of the

GaN HEMT switch can be expressed as

$$C_{\rm g} = C_{\rm gs} = C_{\rm gd} = \frac{{\rm Re}(Y_{11}+Y_{12})}{2{\rm Im}(Y_{11}+Y_{12})\omega r_{\rm g}}, \tag{11}$$

$$C_{\rm ds} = -\frac{\left(\dfrac{2\omega^3 C_{\rm g}^3 r_{\rm g}^2}{1-4r_{\rm g}^2\omega^2 C_{\rm g}^2} + {\rm Im}(Y_{12})\right)}{\omega}, \tag{12}$$

$$R_{\rm ds} = \frac{1}{{\rm Re}(Y_{11}) - \dfrac{3\omega^2 C_{\rm g}^2 r_{\rm g}^2}{1-4r_{\rm g}^2\omega^2 C_{\rm g}^2}}. \tag{13}$$

The introduction of the blocking resistor during the extraction of the intrinsic parameters in the GaN HEMT switch adds another two equations about the intrinsic elements. Four equations correspond to four unknowns. Figure 10 shows the results of the intrinsic parameters extracted via Eqs. (2)–(4). The intrinsic elements at on and off states are different. All the intrinsic parameters shown in Fig. 10 remain almost constant with frequency. This is because of an accurate extraction of all extrinsic elements. Table 2 outlines a selection of the extracted values for on and off states.

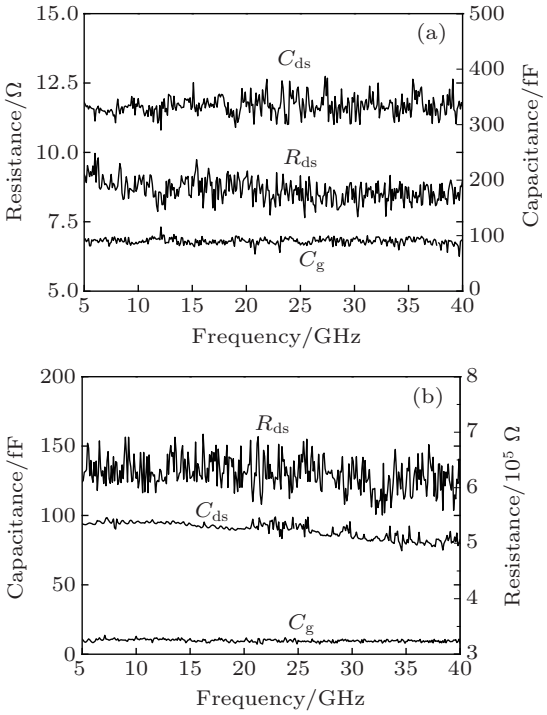


Fig. 10. Extracted $C_{\rm ds}$, $R_{\rm ds}$, $C_{\rm g}$ versus frequency: (a) on state, (b) off state.

Table 2. Intrinsic elements of GaN HEMT switch with gate size of 4×100 μm.

State	$C_{\rm ds}$/fF	$C_{\rm gs}$/fF	$C_{\rm gd}$/fF	$R_{\rm ds}$/Ω
On state	326	84.5	84.5	8.52
Off state	87.4	16.2	16.2	0.61M

4. Results and discussion

The process described above has been used to model the GaN HEMT switch over a frequency range from 5 GHz to 40 GHz. The devices have 0.25 μm gate length, 100 μm finger pitch, and 200 μm, 400 μm, or 800 μm gate size. Furthermore, the CG GaN HEMT switch has a geometric symmetry which is reflected in the observation that $S_{11} \approx S_{22}$ and $S_{12} \approx S_{21}$. Figure 11 shows a comparison of S parameters between the simulation and the measurement at on and off states in Smith charts. The error percentage between the measured and the modeled S parameters is given by the following expression:[25]

$$E_{xy}|_{y=1,2}^{x=1,2} = \sqrt{\frac{\sum_m \sum_n |S_{xy}^{\rm sim} - S_{xy}^{\rm mesa}|^2}{\sum_m \sum_n |S_{xy}^{\rm mesa}|^2}} \times 100\%, \tag{14}$$

where m and n denote the numbers of bias and frequency points, respectively.

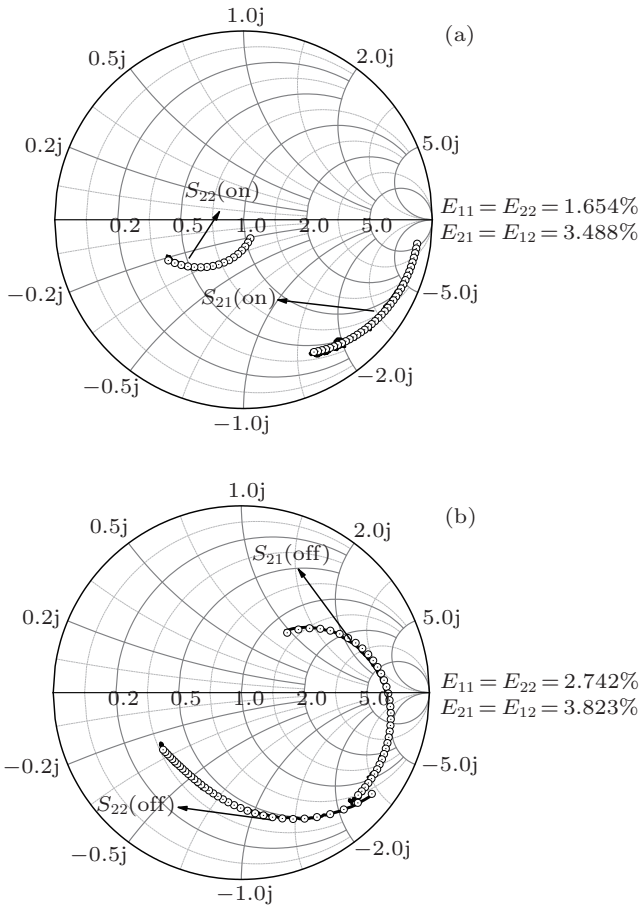


Fig. 11. Comparisons of S-parameters between measurement (—) and simulation (○) in a frequency range of 5–40 GHz for a device with gate size of 4×100 μm: (a) S_{21}, (b) S_{22}.

The agreement between the measured and the modeled S parameters is very good. The percentage errors E_{ij} between the measured and the modeled S_{ij} parameters are within 3.85%. As we know, the S parameters of the GaN HEMT switch are changed with the gate size. In the actual MMIC design, an optimum gate width is determined according to the need of circuit performance. Therefore, we model the switching devices with different gate sizes, and outline their intrinsic parameters at on and off states in Table 3. By analyzing

the modeling results, the quantitative variation of the parameters in the switching model with the gate size is found. Table 4 lists the error percentage of different size GaN HEMT switches, which exhibits a low-percentage error between the measured and the simulated S parameters ($E_{11} = E_{22} < 3.5\%$, $E_{12} = E_{21} < 3.83\%$).

Table 3. Intrinsic parameters of GaN HEMT switches with different sizes.

W_g/μm	C_{ds}(on)/fF	C_{gs}(on)/fF	C_{gd}(on)/fF	R_{ds}(on)/Ω	C_{ds}(off)/fF	C_{gs}(off)/fF	C_{gd}(off)/fF	R_{ds}(off)/MΩ
2×100	214.6	46.24	46.24	15.61	53.5	9.37	9.37	0.52
4×100	326	84.5	84.5	8.52	87.4	16.2	16.2	0.61
8×100	565.18	197.2	217.2	3.36	152.2	31.6	31.6	0.932

Table 4. The error percentage of different size GaN HEMT switches.

W_g/μm	E_{11}		E_{12}		E_{21}		E_{22}	
	On state	Off state	On state	Off state	On state	Off state	On state	Off state
2×100	1.654%	2.742%	3.488%	3.823%	3.488%	3.823%	1.654%	2.742%
4×100	2.413%	3.462%	3.114%	1.879%	3.114%	1.879%	2.413%	3.462%
8×100	1.893%	2.478%	2.697%	3.658%	2.697%	3.658%	1.893%	2.478%

As can be seen from the extracted parameters, with the increase of the gate width, the on state resistance ($R_{on} = R_s + R_{ds} + R_d$) decreases, and the cut-off capacitance ($C_{off} = C_{gs} + C_{ds} + C_{gd}$) increases. The on state resistance R_{on} directly affects the insertion loss, while the cut-off capacitance C_{off} affects the isolation. There is no certain relationship between the cut-off resistance R_{off} and the gate size. This is because when R_{off} is larger than a certain value, its influence on the performance of the switch can be ignored. The product of $R_{on} \cdot C_{off}$ is constant and independent of the total transistor gate size.

The circuit topology and micrograph of an x-band SPDT switch are shown in Fig. 12. The switch has been designed with a linear scalable model of the GaN HEMT switch, with gate periphery equal to 400 μm (4×100 μm), to achieve low insertion loss and high power capacity in the entire bandwidth. As illustrated in Fig. 12(a), the three shunt transistors (Fet1, Fet2, and Fet3) in port 2 are biased opposite to the three shunt transistors (Fet4, Fet5, and Fet6) in port 3, one at zero gate bias and the other at a negative bias smaller than the transistor pinch-off voltage. A micrograph of the fabricated x-band SPDT switch, with overall dimensions of 1.57 mm×1.2 mm, is shown in Fig. 12(b).

The comparisons between the simulated and the modeled results of insertion loss and isolation are presented in Fig. 13. In particular, the insertion loss is lower than 1.116 dB and the isolation is better than 32.126 dB in the whole bandwidth. There is a very good agreement between the simulated and the modeled results. The biggest error between the simulated and the modeled insertion loss and isolation are 0.106 dB and 1.051 dB, respectively. In conclusion, this linear switch-HEMT is useful to predict the performance of the circuits. Despite its simplicity, it is quite useful for rapid designs. This is important when using a MMIC fabrication process, which is being actively developed.

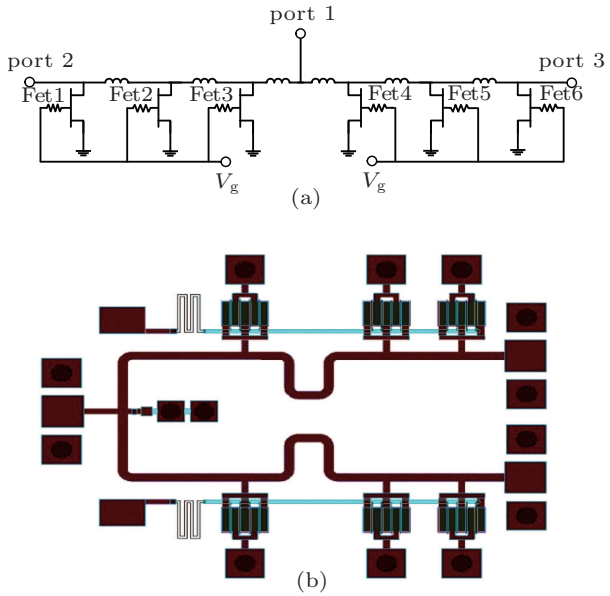


Fig. 12. (color online) (a) Circuit topology and (b) micrograph of the x-band AlGaN/GaN SPDT power switch.

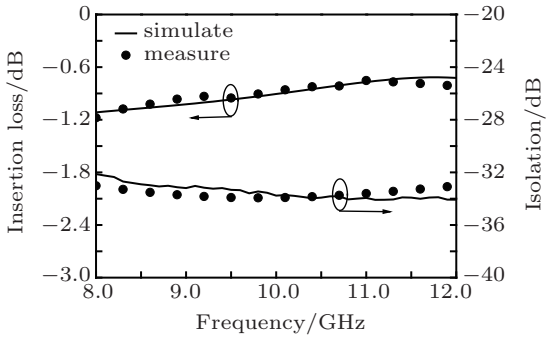


Fig. 13. Simulated and modeled insertion loss and isolation of the x-band switch.

The small-signal equivalent circuit model for understanding the physical structure and predicting small signal S parameters of a device is useful, but it cannot reflect the large signal corresponding RF power harmonic characteristics.[26]

Therefore, the large signal model of the GaN HEMT switch is also of great importance. For the design of switches, the nonlinear model can predict the I–V curves at both positive and negative drain–source voltages, and particularly the continuity of the current in the proximity of $V_{ds} = 0$ V. It can also provide an accurate estimation of the output power as well as the power added efficiency (PAE).[27] As a result, there is a crucial need for developing a dedicated nonlinear model for the GaN HEMT switch from widely used DC and S-parameter measurements, which can be used for successful first-pass design.

5. Conclusion

A novel and accurate direct extraction method of the intrinsic elements of the GaN HEMT switch has been presented. The frequency independence of the extracted intrinsic elements confirms that the intrinsic elements are extracted accurately. This technique is verified through the agreement between the measured and the modeled S-parameters under different bias conditions. Good agreement is obtained between the modeled and the measured results for different gate size HEMTs. The proposed method would be useful for determining the intrinsic elements of the GaN HEMT switches.

Acknowledgements

The authors would like to thank research associate Luo Wei-Jun and professor Ma Xiao-Hua for their helpful guidance, Mr. Li Yan-Kui for his support for the measurement of the GaN HEMT device, and colleagues at my office and fabrication process factory of the Institute of Microelectronics.

References

[1] Drozdovski N V and Caverly R H 2002 *IEEE Transactions on Microwave Theory and Techniques* **50** 4
[2] Bettidi A, Cetronio A, De Dominicis M, Giolo G, Lanzieri C, Manna A, Peroni M, Proietti C and Romanini P 2008 *IEEE Radio Frequency Integrated Circuits Symposium* 329
[3] Chu F T, Chen C, Zhou W and Liu X Z 2013 *Chin. Phys. Lett.* **30** 097303
[4] Tiwat P, Pang L, Yuan T T and Liu X Y 2014 *Chin. Phys. B* **23** 127304
[5] Brady R G, Oxley C H and Brazil T J 2008 *IEEE Transactions on Microwave Theory & Techniques* **56** 1535
[6] Wu Y F, Keller S, Kozodoy P, Keller B P, Parikh P, Kapolnek D, Denbaars S P and Mishra U K 1997 *IEEE Electron Device Lett.* **18** 290
[7] Wu M, Zheng D Y, Wang Y, Chen W W, Zhang K, Ma X H, Zhang J C and Hao Y 2014 *Chin. Phys. B* **23** 097307
[8] Esposto M, Chini A and Rajan S 2011 *IEEE Transactions on Electron Devices* **58** 1456
[9] Campbell C F and Dumka D C 2010 *Microwave Symposium Digest (MTT)* 145
[10] Kharabi F 2012 *Compound Semiconductor Integrated Circuit Symposium (CSICS) IEEE* 1
[11] Pla J A and Struble W 1993 *Microwave Symposium Digest* 641
[12] Shen L, Chen B and Gao J 2014 *International Journal of RF and Microwave Computer-Aided Engineering* **24** 464
[13] Sang L, Xu Y, Chen Y, Guo Y and Xu R M 2011 *Progress in Electromagnetics Research Letters* **20** 27
[14] Lu J, Wang Y, Ma L and Zhi P Y 2008 *Solid-State Electronics* **52** 115
[15] Dambrine G, Cappy A, Heliodore F and Playez E 1988 *IEEE Transactions on Microwave Theory & Techniques* **36** 1151
[16] Pang X F and Shen Y 2008 *Solid-State and Integrated-Circuit Technology ICSICT* 1400
[17] Zhou J, Chang H, Zhang X F, Yang J Z, Zeng Z H, Xu Y, Liu H G, Li Q, Xu W J and Li H O 2014 *Solid-State and Integrated Circuit Technology (ICSICT)* 1
[18] Zhen W B, Li F Q, Li H, Sheng Y, Pan X F and Sheng H C 2008 *Research & Progress of SSE* **28** 372
[19] Gao X B, Du H Y, Wang X Y, Zhao J, Wang T X, Han L H and Gao C Z 2000 *Semiconductor Information* **1** 020
[20] Chen X Y, Xu Q S, Chen J Y, Chen X J, Hao X P, Li F X and Jiang Y Q 2003 *Research & Progress of Solid State Electronics* **2** 013
[21] Liu S, Yao Z, Zhao R and Song X F 2012 *Semiconductor Technology* **37** 347
[22] Campbell C F and Dumka D C 2010 *Microwave Symposium Digest (MTT)* 145
[23] Ren C J, Shen H C, Li Z H, Chen T H, Zhang B and Gao T 2015 *Journal of Semiconductors* **36** 014008
[24] Caddemi A, Crupi G and Donato N 2004 *Microelectronics Journal* **35** 431
[25] Massimo P, Guillermo F, Ahmed A, Giorgio V, Monica B, Enrique S and Dominique S 2005 *ARFTG Conference Digest Spring 65*th
[26] Gao J 2009 *RF and Microwave Modeling and Measurement Techniques for Field Effect Transistors* (New York: SciTech Publisher) pp. 1–346
[27] Jarndal A, Aflaki P, Degachi L, Birafane A, Kouki A, Negra R and Ghannouchi FM 2010 *Solid-State Electronics* **54** 696